Multi-Channel Front-End for Electrochemical Sensing of Metabolites, Drugs, and Electrolytes

Ivan Ny Hanitra, *Student Member, IEEE,* Francesca Criscuolo, Nadezda Pankratova, Sandro Carrara, *Fellow, IEEE,* and Giovanni De Micheli, *Fellow, IEEE*

***Abstract*—A multi-channel front-end for electrochemical sensing is presented. It consists of a multiplexed four-channel readout interface supporting amperometric, voltammetric, and potentiometric measurements. The electronic interface is co-designed according to the target biomarker specifications, and exhibits excellent linearity in both current and voltage sensing. The sensing front-end is characterized with lactate, paracetamol, and lithium sensing, yielding sensitivity of $1.2 \pm 0.3\,\mu$A/mM, $69.6 \pm 2\,$nA/μM, and $55.6\,$mV/decade, respectively. These performances are comparable with the ones obtained with a bulky commercial Autolab potentiostat. Moreover, the limit of detection achieved are of $37 \pm 8\,\mu$M, $2.1 \pm 1.22\,\mu$M, and $11 \pm 3.5\,\mu$M, respectively, for the aforementioned sensors. These values are more than one order of magnitude lower than the relevant detection range. This successful characterization demonstrates the ability of the proposed system to monitor, in a broader sense, metabolites, drugs, and electrolytes. The programmability, versatility and portability of the front-end interface paves the way for a continuous monitoring of different families of biomarkers, suitable for advanced healthcare diagnosis and wearable physiology.**

***Index Terms*—Amperometric sensing, Health care monitoring, Multi-channel electrochemical sensing, Potentiometric sensing, Wearable physiology**

I. Introduction

BIOMEDICAL devices are continuously making steps forward in improving physiology and healthcare monitoring, through wearable technologies or point-of-care devices [1]. Indeed, wearable sensors are ubiquitous in sports applications, where a continuous tracking of physiological status of athletes is crucial to improve their training performance, optimize their resting and hydration routines [2]. For instance, muscle fatigue is assessed through lactate monitoring, given that lactic acid is produced when the metabolism starts lacking energy [3]. Besides, under physical effort, the organism undergoes mineral losses that need to be monitored. Depletion of sodium and potassium levels can lead to dehydration, hypokalemia, hyponatremia, or muscle cramping [4], whereas calcium concentration indicates bone mineral loss [5]. Furthermore, latest biomedical devices contribute to improve healthcare monitoring by providing a fast assessment of health status. Namely, glucose meters are massively deployed in the market, and are vital for subjects suffering from diabetes [6]. In personalized therapy, wearable sensors enable drug dosage control, and its adjustment in real time so that the drug acts in its therapeutic range. For example, lithium is prescribed for people suffering from bipolar disorders, and its intake should be controlled carefully [7].

Electrochemical sensors may provide physiological and health status insights at molecular level, when placed in direct contact with the biological fluid, transducing chemical reactions into electrical signals. Moreover, they are leveraging progresses in microtechnology to be miniaturized and seamlessly integrated into wearable systems [8]. Several wearable and integrated sensing platforms have been reported in literature. Most of them are able to monitor a single biomarker and have an application-specific circuit to readout and control the electrochemical sensor [9] [10]. Nevertheless, in physiology, health status monitoring, and personalized therapy, many biomarkers need to be jointly tracked, providing a more accurate health diagnosis, and because of possible correlation between biological compounds. These compounds might also belong to different family of biomarkers, thus, requiring specific electrochemical sensing techniques. Namely, endogenous metabolites such as lactate are monitored with an enzymatic biosensor biased at a fixed potential and interfaced to an amperometric readout circuit, whereas the detection of exogenous compounds necessitates a voltage scan of the electrochemical cell [11]. As for endogenous electrolytes, they are sensed with an ion-selective sensor interfaced to a potentiometric readout circuit [12]. The four-channel sensing platform presented in [13] enables multi-metabolites and electrolytes sensing, with superior integration level. Yet, it offers neither flexibility nor programmability in the range of biomarkers to be sensed since the architecture does not include a potentiostat. The real-time telemetry system enabling amperometric and potentiometric sensing in [14] provides full-flexibility, programmability and real-time processing, but the overall system is bulky (CMOS front-end, FPGA, transceivers).

In the present work, a four-channel front-end interface (*AmpPot board*) is proposed as a versatile, programmable and wearable solution to enable multi-sensing of different families of analytes that require specific electrochemical sensing techniques. The overall system comprising the electrochemical sensors, the hardware front-end, and the remote control and monitoring unit is detailed in Section II. The circuit architectures implemented for amperometric, voltammetric, and potentiometric measurements are described in Section III. Section IV presents the electrochemical characterization of *Ampot board* with lactate, paracetamol, and lithium sens-

Manuscript submitted on October 8, 2019, revised and accepted on December 11, 2019. This work is supported by H2020 ERC 2014 ADG 669354 CyberCare.

I. Ny Hanitra, F. Criscuolo, N. Pankkratova, S. Carrara, and G. De Micheli are with the Integrated Systems Laboratory (IC-IINFCOM-LSI1), EPFL, Lausanne, CH. (e-mail: ivan.nyhanitra@epfl.ch)

ing. These compounds are typical examples of endogenous metabolite, drug, and electrolyte, that are classes of analyte relevant to be tracked for physiology and advanced healthcare monitoring. Conclusions are reported in Section V.

II. System overview

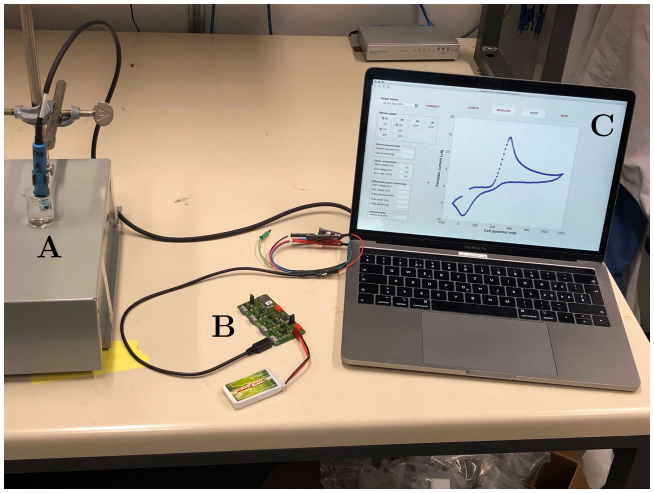

Fig. 1. System setup for in-vitro characterization of paracetamol: **A** Carbon screen-printed electrode in a solution of PBS and controlled concentration of paracetamol; **B** hardware front-end powered by Li-ion battery; **C** GUI to configure the measurements and to acquire voltammograms.

The sensing system comprises three main features: the electrochemical sensors properly functionalized to detect the target biomarker; the electronic interface ensuring the readout and processing of the transduced signal; a remote terminal that programs the multi-sensing platform and collects the data output by the biosensors. The typical setup for in-vitro electrochemical characterization is illustrated in Fig. 1, for paracetamol detection, highlighting the aforementioned features. In the present work, commercial *Screen-Printed Electrodes* (SPEs) are used as support for the developed sensors, and they are interfaced to the hardware through shielded cables.

A. Electrochemical sensors

The proposed system enables metabolites monitoring, drugs detection and quantification, and electrolytes sensing. Electrochemical sensors are developed for lactate, paracetamol, and lithium ions monitoring, these compounds being examples of the aforementioned families of biomarkers. An enzymatic biosensor is required for lactate monitoring, entailing a sensor functionalization with its corresponding enzyme. Paracetamol (acetaminophen, APAP) is an electroactive compound, thus, it could be detected directly with a bare electrode. As for lithium sensing, the sensing electrode is properly functionalized to ensure selectivity and ion-to-electron transduction.

1) Chemicals: Lactate Oxidase (LOx) from aerococcus viridans in powder form of 67.6 units/mg, Lithium L- Lactate (salt, 95%), Acetaminophen (APAP) in powder form, *phosphate-buffered saline* (PBS, pH 7.4) tablets, and all other compounds were purchased from Sigma-Aldrich (Switzerland). *Hydroxymethylferrocene* (HMF, crystalline form, 97%) was obtained from Alfa Aesar (Germany).

Stock solution of 10 mM PBS was prepared by dissolving 1 tablet of PBS in 200 mL of ultra pure water. Stock solution of LOx was prepared by dissolving 0.8 mg of the LOx powder in 160 μL of PBS, and stored at $-18\,^{\circ}$C. Stock solution of 0.5 M L-Lactate was prepared by dissolving 1.40 g of L-Lactate powder in 0.5 mM HMF dissolved in PBS solution. Stock solution of 30 mM APAP was prepared by dissolving 5 mg of APAP powder in 1 mL of PBS.

2) Electrode functionalization for lactate monitoring: Carbon SPE from Metrohm (Switzerland), with an active area of 12.56 mm^2, was used as substrate. A conditioning procedure similar to the one described in [15] was performed. Namely, the electrodes were activated by applying a fixed potential of $+2.0$ V for 5 s, in 0.1 M H_2SO_4, followed by a fixed potential of -0.35 V for 10 s. Then, potential sweeps from -0.3 V to 1.5 V were applied with a scan rate of 5 V/s during 2 min. A final cyclic voltammogram from -0.3 V to 1.5 V at 0.1 V/s was recorded to assess the cleanliness of the electrode. After that, the SPE was rinsed with water. Direct adsorption of the enzyme was carried out by drop-casting 6.3 μL of the stock solution of LOx on top of the electrode. The excess of enzyme was removed by fast dips into deionized water. The sensor was kept overnight at $4\,^{\circ}$C.

3) Electrode functionalization for lithium sensing: Platinum SPE from Metrohm (Switzerland), with an active area of 12.56 mm^2, was used as substrate. The *ion selective membrane* (ISM) was prepared by dissolving 100 mg of mixture consisting of 28.00wt% Poly(vinyl chloride) high molecular weight, 1wt% Li Ionophore VI (6,6-Dibenzyl-1,4,8-11-tetraoxacyclotetradecane), 0.7wt%, Potassium tetrakis(4-chlorophenyl)borate, and 70.3wt% 2-Nitrophenyl octyl ether in 1 mL of Tethraydrofuran (THF). Then, 10 μL of the latter solution was drop-casted on the electrode that was beforehand nanostructured following [16].

B. Hardware front-end

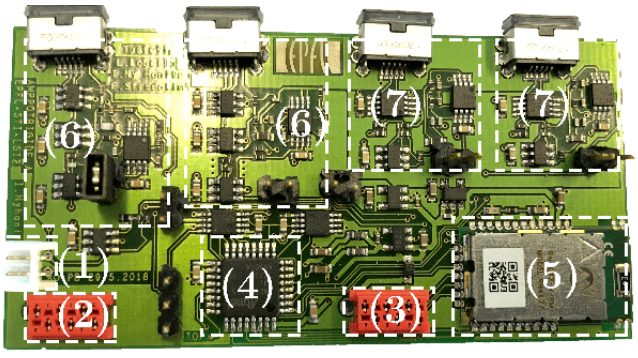

Fig. 2. Different blocks constituting *AmpPot board*: (1) power supply socket, (2) programming/debugging interface, (3) UART/I^{2}C serial ports, (4) microcontroller unit, (5) Bluetooth module, (6) amperometric readout blocks, (7) potentiometric readout blocks.

Electronic front-end based on flexible technology was investigated in [17]. The hardware was successfully characterized, but it had a limited lifespan because it could withstand a limited amount of bendings while worn on body. Therefore, a smaller hardware front-end of 38 $\times$ 76 mm size, mounted

TABLE I
HARDWARE FRONT-ENDS ENABLING MULTI-CHANNEL AMPEROMETRIC AND POTENTIOMETRIC SENSING

	[14]	[13]	**this work**
Electrochemical sensing techniques supported	Amperometric and potentiometric	Amperometric and potentiometric	Amperometric, voltammetric, and potentiometric
Target biomarkers	Nitrite and pH	Lactate, glucose, potassium, and sodium	Lactate, APAP, and lithium
Number of channels	Amperometric (2), potentiometric (2)	Amperometric (2), potentiometric (2)	Amperometric (2), potentiometric (2)
Hardware size (mm)	$58 \times 87 \times 30$	n.a.	$38 \times 76 \times 1.6$
Technology	0.18 μm CMOS (potentiostat and readout) FPGA (MCU)	Flexible PCB	FR4 PCB
Potentiostat	Control amplifier + feedback resistor	None	Control amplifier
Waveform generator	None	None	DDS[1] architecture
Current readout	DDA[2]	Transimpedance amplifier	Transimpedance amplifier
OCP[3] readout	DDA[2]	Buffered and differential circuitry	Buffered and differential circuitry
Power consumption (sensing mode)	157.25 mW	n.a.	150 mW

[1] Direct digital synthesizer [2] Differential difference amplifier [3] Open circuit potential

on a 1.6 mm double side FR4 substrate, is proposed in this work. The different blocks constituting the readout front-end are highlighted in Fig. 2, where circuit blocks (6) represent the two amperometric channels S1 and S2, whereas circuit blocks (7) are the potentiometric channels S3 and S4. A low-power ATxmega32E5 *microcontroller unit* (MCU) is the control and processing unit. It embeds a two-channel 12-bit 12 Msps *digital-to-analog converter* (DAC), and three 16-bit timer/counters, used to drive the three-electrode electrochemical cells. The central unit has a built-in 12-bit *analog to-digital converter* (ADC) enabling multiplexed measurements. Simultaneous measurements are implemented by scanning and sampling the 4 channels at 300 ksps. In addition, the MCU has several serial ports available. The UART module features full-duplex connectivity allowing the user to configure the electrochemical sensing measurements, in one hand, and to collect the processed data relayed by the on-board Bluetooth transceiver, on the other hand. A serial UART line is available to connect the board to a personal computer via a RS-232 cable. An I^2C port is available as well. Lastly, a 3.7 V lithium-ion battery with a capacity of 1100 mAh is powering the hardware. Low-dropout voltage regulators with low quiescent current (25 μA) are used to provide stable 3.3 V to the rail-to-rail operational amplifiers in the analog circuits, to the MCU, and to the Bluetooth module. The power consumption of the overall system is of 135 mW in idle mode, and of 150 mW in sensing mode. Table I compares the features of the hardware front-end proposed and work done in multi-channel amperometric and potentiometric sensing, highlighting the versatility, programmability, and portability of the presented system.

C. Wireless control and monitoring

The on-board dual mode RN4677 *Bluetooth Low Energy* (BLE) 4.0 module is used to establish a wireless communication between the hardware and a remote interface. It features a transparent UART profile to enable serial data connectivity. Namely, it acts as a data pipe between the monitor and the sensing platform by emulating a standard UART protocol. Serial communication is carried out at 115'200 baud rate, with start and stop tags in order to ensure safe data transmission.

A *graphical user interface* (GUI) is developed in Matlab®, and run on a personal computer in the vicinity of the hardware system during electrochemical sensing. Through the graphical interface, the user can configure the multi-sensing platform, and collect data transmitted by the board. The features of the GUI includes establishing a serial connectivity with the target hardware, configuring the sensing channels with the parameters of the measurements, requesting the start/pause/resume/stop of the measurement, and exporting data as text files. The collected data are displayed on the GUI in real time at 276 sps.

III. CIRCUIT ARCHITECTURE

In this section, the analog front-end circuitry for amperometric and potentiometric measurements are described.

A. Amperometric readout

The detection of the target analyte at the sensing electrode triggers redox reactions that transduce the chemical reaction into an electrical current. Controlled-voltage techniques are the most common approaches for the characterization of Faradaic processes [18] [19]. The overall circuit for amperometric readout is displayed in Fig 3.

A three-electrode electrochemical cell in a grounded *working electrode* (WE) configuration is implemented. The cell potential E_{cell} is applied between the sensing electrode WE and the *reference electrode* (RE), while the Faradaic current is measured in the path from WE to the *counter electrode* (CE). Namely, the latter electrode is closing the current path by balancing the electron transfer observed at the sensing

This article has been accepted for publication in a future issue of this journal, but has not been fully edited. Content may change prior to final publication. Citation information: DOI 10.1109/JSEN.2019.2959885, IEEE Sensors Journal

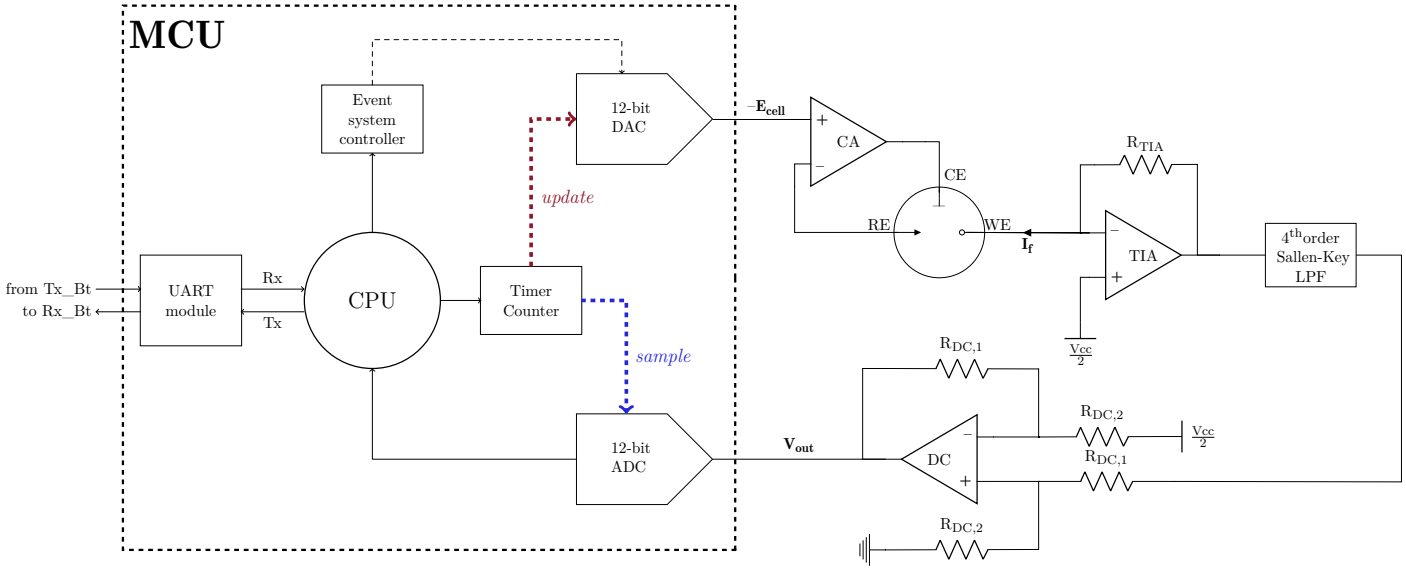

Fig. 3. Circuit architecture for electrochemical cell stimulation and Faradaic current readout. The full-duplex UART communication enables remote configuration of the electrochemical sensing measurements and transmission of the sampled and structured data to the remote terminal.

electrode. In such configuration, RE is a high impedance node so that its potential is not altered by Faradaic processes. The control amplifier *CA* serves as potentiostat to achieve the aforementioned conditions.

Current-to-voltage conversion is adopted to process redox currents. *Trans-impedance amplifiers* (TIAs) with a feedback resistor appear to be a simple and efficient approach [20] [21]. The dynamic range of the amperometric measurement is set by the feedback resistor. Gain of $30\,\mathrm{k\Omega}$ is used so that currents of $[-30; 30]\,\mu\mathrm{A}$ are sensed, which correspond to the typical current range of the metabolites and drugs of interest [22]. Resistors of $0.1\,\%$ tolerance are used. Moreover, an offset of $\frac{V_{cc}}{2}$ is applied at the non-inverting input of the TIA, enabling bi-directional current measurements. The signal conditioning block comprises a 4^{th}order Sallen - Key *low-pass filter* (LPF), with a $-3\,\mathrm{dB}$ cut-off at $200\,\mathrm{Hz}$, since after applying a potential to the cell, the Faradaic current needs at least $10\,\mathrm{ms}$ to stabilize. A high-order filter is chosen to attenuate high frequency noise and interference. It serves as anti-aliasing element as well. Furthermore, the opamp *DC* is used to compensate the offset of $\frac{V_{cc}}{2}$ introduced by the TIA, in order to use the full dynamic range of the ADC. By sizing the resistors properly, the channel output voltage is $V_{out} = 1 + R_{TIA} \cdot I_f\,[V]$. Low-noise, low-distortion, rail-to-rail MAX4475 operational amplifiers are used. The front-end architecture is replicated for amperometric channels S1 and S2.

B. Voltammetric techniques

Different amperometric techniques could be implemented to characterize the electrochemical sensor, depending on the voltage E_{cell} applied by the potentiostat. Namely, potential steps, potential sweeps, or potential pulses can be used to polarize the cell [23]. In the present sensing front-end, *chronoamperometry* (CA), *cyclic voltammetry* (CV), and *differential pulse voltammetry* (DPV) are implemented. CA involves a potentiostatic sensing for which a fixed potential is applied to the cell during the whole measurement. This is done by writing the corresponding digital code to the DAC of the MCU, and feeding it to the potentiostat. As for voltammetric techniques, a continuous and programmable waveform generator is needed to support multi-mode waveforms. A *direct digital synthesizer* (DDS) is typically implemented to output periodic waveforms [24]. It is a mixed-mode circuit using a digital controller and a DAC. As shown in Fig. 3, a 16-bit Timer/Counter of the MCU is the time reference for both generation of the correct waveform, and synchronization of the ADC that samples the output voltage. The module is clocked at $250\,\mathrm{kHz}$ with the peripheral clock. The *event system controller* is used to trigger DAC conversions every $1\,\mathrm{ms}$. The latter module is synchronized with the Timer/Counter. The 12-bit DAC outputs the analog cell potential with an LSB of $0.8\,\mathrm{mV}$.

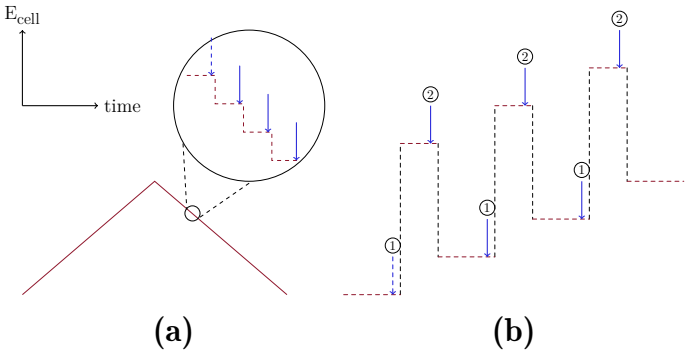

Fig. 4. Waveform applied to the electrochemical cell with a DDS architecture: **(a)** triangular voltage sweep for CV, **(b)** pulse-modulated voltage for DPV. The blue arrows indicate the instant when the ADC samples the channel output voltage.

Typical waveforms for CV and DPV measurements are displayed in Fig. 4. The proposed DDS generates upwards and downwards staircase voltages, achieving scan rate (slope

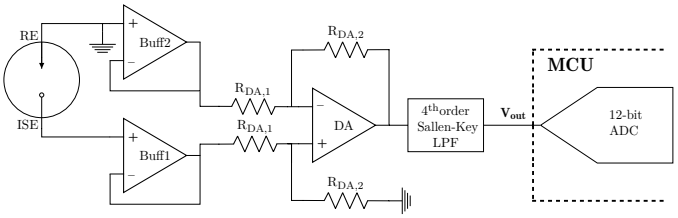

Fig. 5. Circuit architecture for potentiometric readout.

of the triangular waveform) from 8 mV/s to 2 kV/s. Likewise, pulsed-voltammetry is implemented with programmable pulse amplitude, width, and period. In this case, the Faradaic current is sampled twice: first, before applying the pulse, secondly, just before applying the next base potential $E_{b,n+1}$. The differential current $\delta I_{f,n} = I_{f2,n} - I_{f1,n}$ is computed on-board, and the couple $(E_{b,n}, \delta I_{f,n})$ is sent to the user terminal.

C. Potentiometric readout

The readout circuitry for potentiometric sensing channels is displayed in Fig. 5. The *open circuit potential* (OCP) of the cell is measured by sensing the floating potential of the *ion selective electrode* (ISE) against the grounded RE. The latter is shared between the two potentiometric channels. High impedance voltage buffers are needed to achieve open circuit conditions. Thus, MAX44242 voltage buffers that draw up to 0.5 pA bias current are used. This non-zero polarization current is required to reduce potential drift of the sensor, improve its lower *limit of detection* (LOD), and to increase sensor sensitivity [25]. Next, the differential signal is sensed and amplified with the opamp *DA*. A gain of 3.9 is chosen so that the full dynamic range of the ADC is used, given that the sensor OCP vary in $[0; 500]$ mV. This differential sensing stage reduces common-mode interference as well. Next, the signal conditioning path includes a 4^{th} order Sallen-Key LPF similar to the one previously described. The filtered channel output voltage is sensed by the built-in ADC of the MCU. The front-end architecture is replicated for potentiometric channels S3 and S4.

D. Electrical characterization

TABLE II
ELECTRICAL CHARACTERISTICS OF AMPEROMETRIC AND POTENTIOMETRIC CHANNELS

	Amperometric channels	**Potentiometric channels**
Input range	$[-33; +33]$ μA	$[50; 530]$ mV
Sensitivity/Gain	29.92 ± 0.04 mV/μA	3.89 ± 0.05
	$R^2 > 0.9999$	$R^2 > 0.9999$
SNR @ V_{out}	96.2 dB	105.4 dB
Resolution	320 nA	1.3 mV
Integrated noise @ 100 Hz (simulated)	6.3 nA	84.2 μV

The amperometric channels are characterized first in terms of linearity by applying a DC current between $-40\,\mu$A and $40\,\mu$A at the WE node. The transduced voltage is measured at the output node and plotted in Fig. 6, exhibiting an excellent

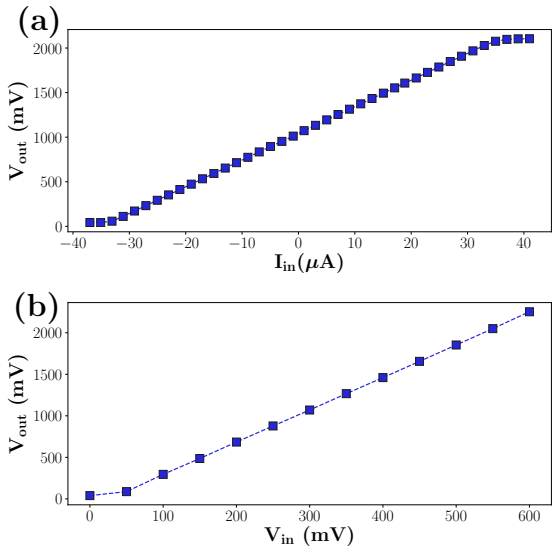

Fig. 6. Electrical characterization of **(a)** amperometric and **(b)** potentiometric channels.

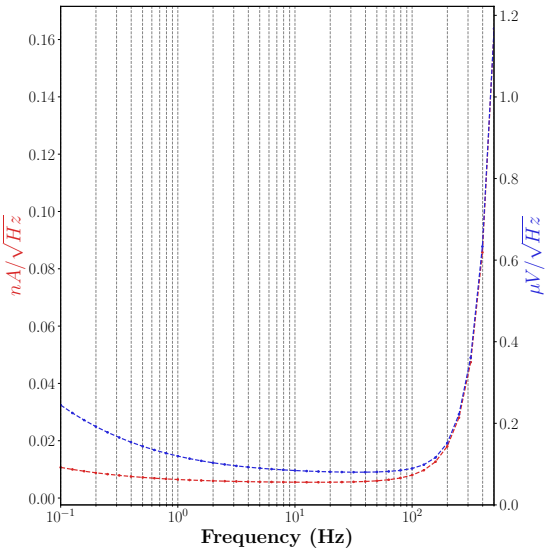

Fig. 7. Simulated input-referred noise of amperometric (*red*) and potentiometric (*blue*) channel. The signal bandwidth is of 100 Hz.

linearity, where sensitivity of 29.92 mV/μA corresponds to the gain of the transimpedance amplifier. The *signal-to-noise ratio* (SNR) is measured at the output node. A resolution of 320 nA is computed, taking into account the noise level. As for potentiometric channels, a DC voltage between 0 mV and 600 mV is applied between ISE and RE terminals. The output voltage is measured and plotted in Fig. 6, showing an excellent linearity. Sensitivity of 3.89 corresponds to the gain of the differential amplifier. The SNR is measured at the output node, and a resolution of 1.3 mV is obtained, taking into account the noise level. The simulated input-referred noise spectrum of both amperometric and potentiometric channels is plotted in Fig. 7, with the PSpice models of the operational amplifiers used. The integrated noise at 100 Hz is of 6.3 nA, for the current-sensing channel, and of 84.2 μV, for the OCP-

sensing channel. The electrical features of both amperometric and potentiometric channels are summarized in Table II.

IV. Electrochemical sensing

The ability of the described electrochemical sensing front-end to monitor endogenous metabolites, exogenous compounds, and electrolytes is validated with lactate monitoring, paracetamol detection, and lithium ion sensing, respectively. An Autolab potentiostat (Metrohm, Switzerland) driven by Nova 1.11 software is a reference tool used during the development and characterization of electrochemical sensors. In this work, it is used for performance comparison with *AmpPot board*.

A. Lactate monitoring

The lactate sensor was described in Section II-A2. LOx catalyzes the reduction of L-Lactate into pyruvate, where HMF was used as redox mediator, involving ferrocene—ferrocenium ($Fc|Fc^+$) redox couple. A Ag/AgCl double-junction RE (Metrohm, Switzerland) was used.

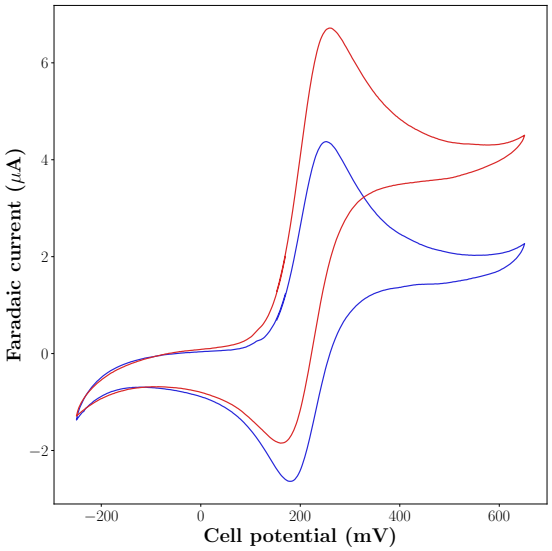

Fig. 8. CV responses at 10 mV/s of LOx-C lactate biosensor, in 10 mM PBS solution containing 0.5 mM HMF: without L-Lactate (*blue*), with 4.95 mM L-Lactate (*red*).

The catalytic activity of the enzymatic biosensor was assessed with a CV measurement between -250 mV and 650 mV, at slow scan rate (10 mV/s). The CV was carried out, first, in a background solution of 10 mM PBS and 0.5 mM HMF, then in presence of 4.95 mM L-Lactate. The resulting cyclic voltammograms are displayed in Fig.8. The blue CV plot shows the redox response of $Fc|Fc^+$ couple in aqueous solution, highlighting a reversible reaction with oxidation potential around 260 mV and reduction potential around 190 mV. In presence of 4.95 mM L-Lactate, the anodic current is increased of 2.8 μA, whereas the cathodic current is decreased of 1.6 μA. Similar results were obtained in [15], where anodic current sensitivity of 0.56 μA/mM was obtained. This analysis confirms the well-functioning of the directly adsorbed enzyme in the catalytic response of the lactate biosensor.

Next, the analytical properties of the designed lactate biosensor were assessed with CA measurements. A fixed potential of 300 mV was applied to the electrochemical cell, slightly above the oxidation potential of the mediator. The background solution consisted of 10 mM PBS with 0.5 mM HMF. The stock solution containing 0.5 M L-Lactate and 0.5 mM HMF in 10 mM PBS was gradually injected, maintaining the concentration of mediator in solution constant.

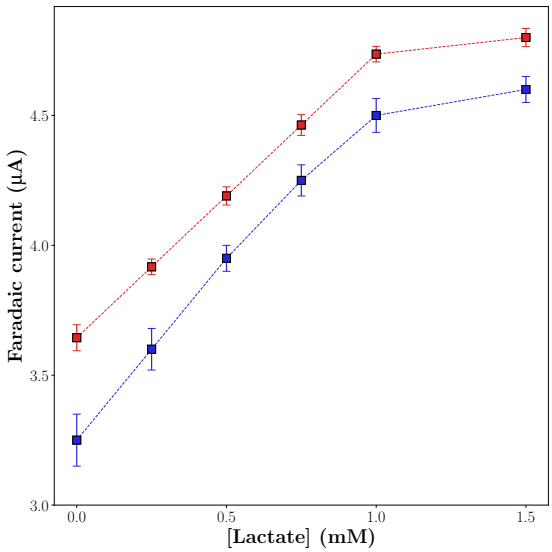

Fig. 9. Calibration curves obtained from CA measurement of LOx-C lactate biosensor at $E_{cell} = 300$ mV: with *AmpPot board* (*blue*), with an Autolab potentiostat (*red*). The error bars correspond to standard deviations obtained with three measurements, with different sensors.

The calibration curve of lactate monitoring is displayed in Fig. 9 (blue plot). The biosensor exhibits a sensitivity of 1.2 ± 0.3 μA/mM up to 1 mM. The LOD is computed as the concentration of L-Lactate that gives an oxidation current three times the standard deviation of the background current. LOD of 37 ± 8 μM is obtained. Similar experiments were done with an Autolab potentiostat (Fig. 9, red plot). The analytical performance of the designed biosensor are reported in Table III. Measurements carried out with *AmpPot board* result in slightly higher sensitivity, but higher LOD compared to the commercial potentiostat. Indeed, a higher background current noise is observed with the proposed system, but the LOD is acceptable considering that the physiological relevant level of lactate is of $2 - 30$ mM [13].

TABLE III
Performance of Sensing Front-End on Developed Lactate Biosensor

	AmpPot board	Autolab
Sensitivity (μA/mM)	1.2 ± 0.3	1.08 ± 0.12
Linear response (mM)	up to 1	up to 1
	R=0.99	R=0.99
Limit of detection (μM)	37 ± 8	20.6 ± 3.6

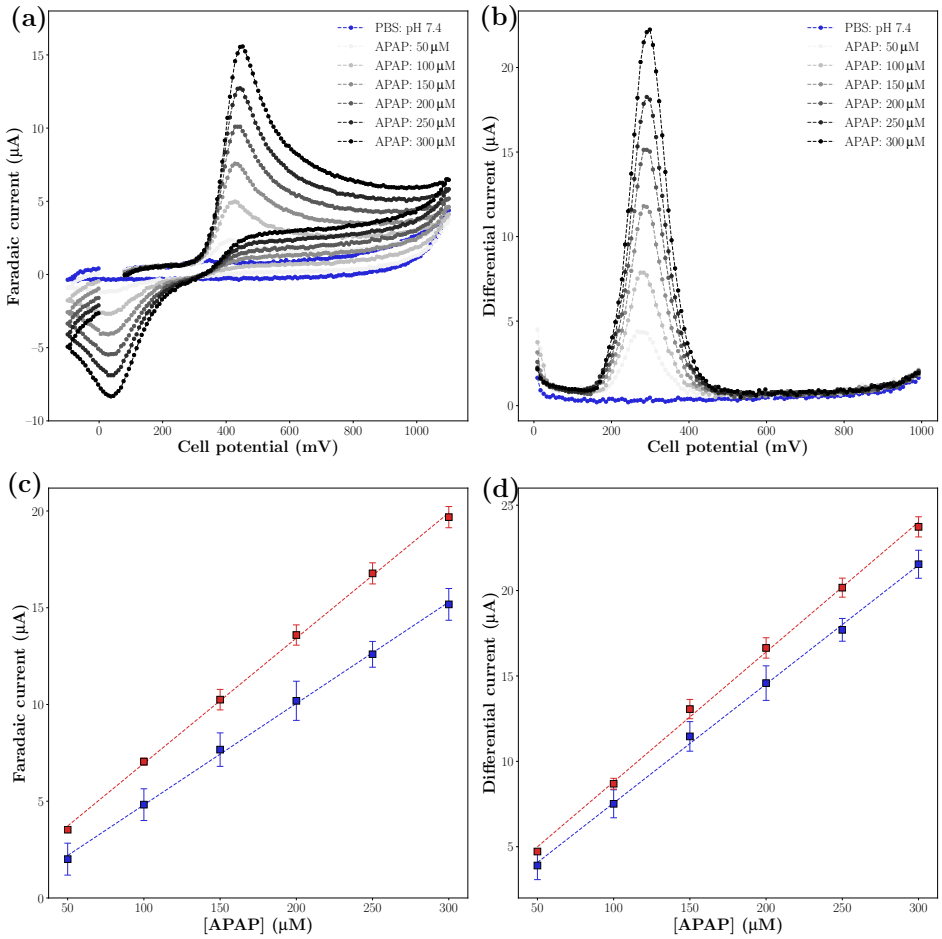

Fig. 10. Electrochemical detection of paracetamol with *AmpPot board*: **(a)** cyclic voltammograms run at 0.1 V/s; **(b)** differential pulse voltammograms; calibration of **(c)** CV measurements and **(d)** DPV measurements with *AmpPot board* (blue) and Autolab potentiostat (red). The error bars correspond to standard deviations obtained with three measurements, with different sensors.

B. Paracetamol detection

In the following, the proposed system is validated with APAP detection. Voltammetric techniques were used to characterize the sensor that consists of bare carbon SPE from Metrohm-Switzerland (carbon circular WE of 12.56 mm^2 active area, carbon CE, silver RE). Measurements were performed in 10 mM PBS background electrolyte. APAP calibration was performed from 50 to 300 μM with both CV and DPV. The parameters of the triangular and pulse-modulated waveform are displayed in Table IV, similar to the one used in [22]. These parameters could be optimised, in particular, by tuning the sampling frequency in order to reduce the power consumption during voltammetric measurements [26].

TABLE IV
PARAMETERS OF VOLTAMMETRIC WAVEFORMS

Cyclic voltammetry		**Differential pulse voltammetry**	
Lower potential	−0.1 V	Lower potential	0 V
Upper potential	1.1 V	Upper potential	1 V
Step potential	8.1 mV	Step potential	8.1 mV
Scan rate	0.1 V/s	Pulse amplitude	80 mV
		Pulse duration	80 ms
		Pulse period	160 ms

The voltammograms of the calibration of paracetamol detection with *AmpPot board* are displayed in Fig. 10. For CV measurements, the peak oxidation currents are obtained around 430 mV, and increase linearly with APAP concentration. A sensitivity of 52.4 ± 0.15 nA/μM is obtained with good linearity. The LOD is computed as the concentration of APAP providing a Faradaic current three times the standard deviation of the background current in a potential window around the peak oxidation current. LOD of 2.6 ± 0.49 μM is obtained, below the concentration range at which toxicity is detected (20 μM, [27]). As for APAP calibration through DPV measurements, the differential Faradaic current peaks are around 290 mV. A higher sensitivity of 64.7 ± 2.76 nA/μM is achieved because the differential measurements reduce the contribution of background currents arising from interfacial capacitance or non-Faradaic processes [23]. The results obtained with *AmpPot board* are compared with the ones obtained with an Autolab potentionstat. Table V sums up the comparison, putting in evidence comparable sensitivity and LOD with both voltammetric techniques. The slightly lower sensitivity observed with the proposed hardware is due to an higher current background noise arising from the cabling of the hardware to the biosensor in such in-vitro characterization. As

TABLE V
PERFORMANCE OF SENSING FRONT-END ON PARACETAMOL DETECTION

	AmpPot board		Autolab		[22]	
	CV	DPV	CV	DPV	CV	DPV
Sensitivity (nA/μM)	52.4 ± 0.15	69.6 ± 2.0	64.7 ± 2.76	76.0 ± 5.83	40	22
Root Mean Squared Error (μA)	0.146	0.226	0.149	0.269	n.a.	n.a.
Coefficient of determination, R^2	0.9989	0.9985	0.9993	0.9983	~ 1	0.98
Limit of detection (μM)	2.6 ± 0.49	2.1 ± 1.22	0.75 ± 0.42	0.5 ± 0.15	n.a.	n.a.

a comparison with literature, the system developed provides much better sensitivity than in [22], where sensitivities of 40 nA/μM and 22 nA/μM were obtained, with CV and DPV, respectively.

C. Lithium sensing

The characterization of the potentiometric channels of *AmpPot board* was performed with lithium sensors. The measurements were done in water samples. LiCl was gradually injected from 10^{-8} M to 10^{-1} M, every 50 s, and the OCP between the ISE and a Ag/AgCl double junction electrode (Metrohm, Switzerland) was measured. The calibration curve of the lithium sensor is reported in Fig. 11, with the OCP time trace in the inset. Two regions could be distinguished: in diluted LiCl analyte, the OCP increases slightly; above a threshold concentration, the OCP increases linearly, with clear potential steps. A quasi-Nernstian slope of 55.6 ± 1.16 mV/decade is obtained. The lower LOD of the sensor is computed, according to IUPAC definition, as the intersection of the extrapolated linear portions of the calibration curve. A lower LOD of 11 ± 3.5 μM is obtained. This is well below the minimum effective concentration of lithium drug (0.5 mM, [28]). Likewise, lithium sensor calibrations were carried out with an Autolab potentiostat. The obtained calibration measurements are compared in Table VI. The measurements with *AmpPot board* yield lower sensitivity but very good linearity. Besides, the LODs are comparable.

TABLE VI
PERFORMANCE OF SENSING FRONT-END ON DEVELOPED LITHIUM SENSOR

	AmpPot board	Autolab
Sensitivity (mV/decade)	55.6 ± 1.16	61.9 ± 0.48
Root Mean Squared Error (mV)	0.5	0.1
Coefficient of determination, R^2	0.9994	0.9993
Limit of detection (μM)	11.0 ± 3.50	12.4 ± 2.40

V. CONCLUSION

A multiplexed four-channel electrochemical sensing front-end supporting amperometric, voltammetric, and potentiometric sensing is presented. The system is validated with lactate monitoring, paracetamol detection, and lithium sensing, that could be expanded more generally to endogenous metabolites monitoring, exogenous compounds detection, and electrolytes sensing, respectively. The versatility, programmability, and portability of the overall system paves the way for advanced wearable physiology, healthcare monitoring, and personalized therapy. Further development will focus on the realization of a multi-target and integrated electrochemical sensing platform, aiming the sensing of the same families of biomarkers presented in this work.

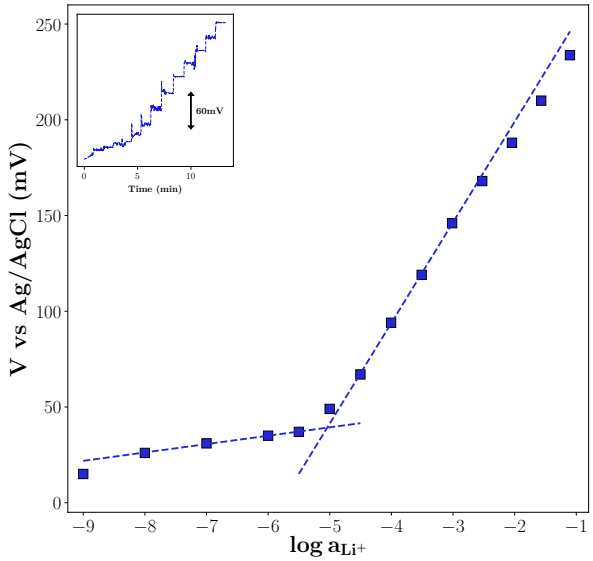

Fig. 11. Lithium sensor calibration in water background electrolyte.

REFERENCES

[1] A. J. Bandodkar, I. Jeerapan, and J. Wang, "Wearable chemical sensors: Present challenges and future prospects," *ACS Sensors*, 2016.
[2] P. Düking, C. Stammel, B. Sperlich, S. Sutehall, B. Muniz-Pardos, G. Lima, L. Kilduff, I. Keramitsoglou, G. Li, F. Pigozzi, and Y. P. Pitsiladis, "Necessary Steps to Accelerate the Integration of Wearable Sensors Into Recreation and Competitive Sports," *Current Sports Medicine Reports*, vol. 17, no. 6, pp. 178–182, 2018.
[3] K. Mitsubayashi, M. Suzuki, E. Tamiya, and I. Karube, "Analysis of metabolites in sweat as a measure of physical condition," *Analytica chimica acta*, vol. 289, no. 1, pp. 27–34, 1994.
[4] D. B. Speedy, T. D. Noakes, and C. Schneider, "Exercise-associated hyponatremia: A review," *Emergency Medicine*, vol. 13, no. 1, pp. 17–27, 2001.
[5] R. Klesges, K. Ward, M. Shelton, and et al., "Changes in bone mineral content in male athletes: Mechanisms of action and intervention effects," *JAMA*, vol. 276, no. 3, pp. 226–230, 1996.
[6] J. Kim, A. S. Campbell, and J. Wang, "Wearable non-invasive epidermal glucose sensors: A review," *Talanta*, vol. 177, pp. 163 – 170, 2018, special issue dedicated to Professor Gary Christian's 80th Birthday.
[7] A. Muneer, "Staging Models in Bipolar Disorder: A Systematic Review of the Literature." *Clinical psychopharmacology and neuroscience : the official scientific journal of the Korean College of Neuropsychopharmacology*, vol. 14, no. 2, pp. 117–30, 2016.
[8] J. Kim, A. S. Campbell, B. E.-F. de Ávila, and J. Wang, "Wearable biosensors for healthcare monitoring," *Nature Biotechnology*, 2019.

[9] J. Dieffenderfer, M. Wilkins, C. Hood, E. Beppler, M. A. Daniele, and A. Bozkurt, "Towards a sweat-based wireless and wearable electrochemical sensor," *Proceedings of IEEE Sensors*, pp. 5–7, 2017.

[10] J. Kim, J. R. Sempionatto, S. Imani, M. C. Hartel, A. Barfidokht, G. Tang, A. S. Campbell, P. P. Mercier, and J. Wang, "Simultaneous Monitoring of Sweat and Interstitial Fluid Using a Single Wearable Biosensor Platform," *Advanced Science*, p. 1800880, 2018.

[11] S. Carrara, A. Cavallini, V. Erokhin, and G. D. Micheli, "Multi-panel drugs detection in human serum for personalized therapy," *Biosensors and Bioelectronics*, vol. 26, no. 9, pp. 3914 – 3919, 2011.

[12] M. Parrilla, M. Cuartero, and G. A. Crespo, "Wearable potentiometric ion sensors," *TrAC - Trends in Analytical Chemistry*, vol. 110, pp. 303–320, 2019.

[13] W. Gao, S. Emaminejad, H. Y. Y. Nyein, S. Challa, K. Chen, A. Peck, H. M. Fahad, H. Ota, H. Shiraki, D. Kiriya, D.-H. Lien, G. A. Brooks, R. W. Davis, and A. Javey, "Fully integrated wearable sensor arrays for multiplexed in situ perspiration analysis," *Nature*, vol. 529, no. 7587, pp. 509–514, 2016.

[14] W. S. Wang, H. Y. Huang, S. C. Chen, K. C. Ho, C. Y. Lin, T. C. Chou, C. H. Hu, W. F. Wang, C. F. Wu, and C. H. Luo, "Real-time telemetry system for amperometric and potentiometric electrochemical sensors," *Sensors*, vol. 11, no. 9, pp. 8593–8610, 2011.

[15] A. Parra, E. Casero, L. Vázquez, F. Pariente, and E. Lorenzo, "Design and characterization of a lactate biosensor based on immobilized lactate oxidase onto gold surfaces," *Analytica Chimica Acta*, vol. 555, no. 2, pp. 308–315, 2006.

[16] F. Criscuolo, I. Taurino, F. Stradolini, S. Carrara, and G. De Micheli, "Highly-stable Li+ ion-selective electrodes based on noble metal nanostructured layers as solid-contacts," *submitted to Analytica Chimica Acta*, 2018.

[17] I. Ny Hanitra, L. Lobello, F. Stradolini, A. Tuoheti, F. Criscuolo, T. Kilic, D. Demarchi, S. Carrara, and G. De Micheli, "A Flexible Front-End for Wearable Electrochemical Sensing," in *IEEE International Symposium on Medical Measurements and Applications, Proceedings*, 2018.

[18] L. Li, X. Liu, W. A. Qureshi, and A. J. Mason, "CMOS amperometric instrumentation and packaging for biosensor array applications," *IEEE Transactions on Biomedical Circuits and Systems*, vol. 5, no. 5, pp. 439–448, 2011.

[19] H. Li, X. Liu, L. Li, X. Mu, R. Genov, and A. J. Mason, "CMOS Electrochemical Instrumentation for Biosensor Microsystems: A Review," *Sensors*, 2016.

[20] S. S. Ghoreishizadeh, C. Baj-rossi, A. Cavallini, S. Carrara, and G. De Micheli, "An Integrated Control and Readout Circuit for Implantable Multi-Target Electrochemical Biosensing," *IEEE Transactions on Biomedical Circuits and Systems*, vol. 8, no. 6, pp. 1–8, 2014.

[21] D. Kim, B. Goldstein, W. Tang, F. J. Sigworth, and E. Culurciello, "Noise analysis and performance comparison of low current measurement systems for biomedical applications," *IEEE transactions on biomedical circuits and systems*, vol. 7, no. 1, pp. 52–62, 2013.

[22] F. Stradolini, A. Tuoheti, P. M. Ros, D. Demarchi, and S. Carrara, "Raspberry Pi Based System for Portable and Simultaneous Monitoring of Anesthetics and Therapeutic Compounds," pp. 237–240, 2017.

[23] A. J. Bard and L. R. Faulkner, *Electrochemical Methods: Fundamentals and Applications*, 2nd ed., J. Wiley, Ed. John Wiley & sons, 2001.

[24] S. S. Ghoreishizadeh, C. Baj-Rossi, S. Carrara, and G. De Micheli, "Nano-sensor and circuit design for anti-cancer drug detection," *Proceedings of the 2011 IEEE/NIH Life Science Systems and Applications Workshop, LiSSA 2011*, pp. 28–33, 2011.

[25] E. Lindner and R. E. Gyurcsányi, "Quality control criteria for solid-contact, solvent polymeric membrane ion-selective electrodes," *Journal of Solid State Electrochemistry*, vol. 13, no. 1, pp. 51–68, 2009.

[26] S. Aiassa, S. Carrara, and D. Demarchi, "Optimized sampling rate for voltammetry-based electrochemical sensing in wearable and iot applications," *IEEE Sensors Letters*, vol. 3, no. 6, pp. 1–4, June 2019.

[27] F. Shihana, D. M. Dissanayake, P. I. Dargan, and A. H. Dawson, "A modified low cost coulorimetric method for paracetamol measurement in plasma," *Clinical Toxicology*, vol. 48, no. 1, pp. 42–46, 2011.

[28] G. Damien, L. Abdelkrim, F. Valérie, T. A. Marie, L. Alain, and C. Marc, *Evaluation of a new lithium colorimetric assay performed on the Dade Behring Dimension® X-pand^{TM} system* , 2004, vol. 42.